

## Detailed-term-accounting approximation calculations of the radiative opacity of aluminum plasmas: A systematic study

Jiaolong Zeng and Jianmin Yuan

*Department of Applied Physics, National University of Defense Technology, Changsha 410073, People's Republic of China*

(Received 7 January 2002; revised manuscript received 13 March 2002; published 12 July 2002)

The spectrally resolved radiative opacity and the Rosseland and Planck mean opacities are calculated by using the detailed-term-accounting approximation for aluminum plasmas with varieties of density and temperature. The results are presented along a 40 eV isothermal sequence, a 0.01 g/cm<sup>3</sup> isodense sequence, and a sequence with average ionization degree  $Z^* \sim 7.13$ . Particular attention is given to the influence of the detailed treatment of spectral lines on the Rosseland mean opacity under different thermodynamical conditions. The results show that at densities of 0.004 g/cm<sup>3</sup> and higher, the opacities are not very sensitive to the spectral linewidth within a reasonable range. As examples, the Rosseland mean opacity, which is most sensitive to the detailed linewidth, at 40 eV and 0.004 g/cm<sup>3</sup> changes no more than 15%, when we change the electron impact spectral linewidth artificially by reducing it by 50% or increasing it twice, and at 40 eV and 0.1 g/cm<sup>3</sup> it changes less than 5%. For comparison, we also carried out calculations by using an average atom model. For the Rosseland mean opacities, the two models show quite large differences, in particular at low densities, while for the Planck mean opacities the results of the two models are much closer.

DOI: 10.1103/PhysRevE.66.016401

PACS number(s): 52.25.Os, 52.20.-j

### I. INTRODUCTION

There has long been of interest in experimental and theoretical determinations of the radiative opacities of high temperature plasmas. This interest is mainly due to the urgent need for radiative opacities for practical applications, fusion research, and plasma diagnostics. The Opacity Project (OP) [1,2] obtained a large number of accurate energy levels and radiative data for opacity calculations for most astrophysical abundant elements. A series of papers was published later collected in the two volume book *The Opacity Project* [3]. Their computations were made using the close-coupling approximation employing the *R*-matrix method. The Iron Project [4] also calculated a large amount of radiative data to obtain the opacity of iron plasmas for the iron atom and ions of different ionization stages. As far as we know, the data obtained by the two projects are the most comprehensive so far.

During the past two decades, aluminum plasmas have been of particular interest. Much experimental and theoretical effort has been made to investigate the opacities through aluminum plasmas. Experimentally, the investigations can be classified into two categories according to the photon energy ranges:  $h\nu \geq 1$  keV and  $h\nu \leq 1$  keV. Most experiments [5–10] have been carried out in the x-ray region ( $h\nu \geq 1$  keV). These experiments measured the x-ray transmission near the photon energy region of the inner-shell excitations of one *1s* electron to the *2p* orbital (the excitation energy is about 1530 eV for Al VIII ions). During the last decade, more and more experiments focused on time-resolved x-ray spectroscopy by using various ultrashort laser pulses or other x-ray sources [11–14]. Compared with the energy range of  $h\nu \geq 1$  keV, less experimental work had been done in the spectral range of  $h\nu \leq 1$  keV. One of the reasons may be that it requires reliable extreme uv diagnostics and sufficient suppression of the self-emission from the

sample. To the best of our knowledge, only one or two experimental studies have been carried out in this spectral range. Winhart *et al.* [15,16] measured the spectrally resolved transmission of an aluminum plasma in local thermodynamic equilibrium (LTE) in the energy range 70–280 eV at a typical temperature of 20 eV and a density of 0.01 g/cm<sup>3</sup>. The main structures observed in their experiment are due to the *2p-3s* transitions caused by Al V and Al VI ions. The contributions caused by *2p-3d* transitions are greatly smoothed by finite spectrometer resolution power. They also compared their experimental data with some theoretical opacity models [17–21]. The success of the experimental studies stimulated the theoretical physicists to further efforts. A lot of theoretical studies [18,22–25] have been carried out to simulate x-ray transmission spectra. Most of them approximated the *K*-shell excited (*1s* hole) states as discrete ones and only took account of Doppler broadening in calculating the line absorption cross sections. Recently, we [26] simulated the x-ray ( $h\nu \geq 1$  keV) transmission through laser-produced aluminum plasmas at the temperatures and densities of 40 eV and 0.0135 g/cm<sup>3</sup> and of 58 eV and 0.02 g/cm<sup>3</sup>, respectively, by using the detailed-term-accounting (DTA) approximation. We [27] have also calculated the radiative opacity (including the Rosseland and Planck mean opacities) in the photon energy range of  $h\nu \leq 1$  keV of an aluminum plasma at a temperature of 20 eV and a density of 0.01 g/cm<sup>3</sup> using the same DTA approximation. The calculated transmissions under the above mentioned conditions agree satisfactorily with the experiments and other theoretical results. We have shown some additional features in calculating the radiative opacity of aluminum plasmas. First, in the  $h\nu \geq 1$  keV region, the autoionization width is one of the major broadening mechanisms and should be considered in obtaining the opacity or transmission. As mentioned above, in the x-ray region  $h\nu \geq 1$  keV, the dominant structures of the opacity or transmission are caused by

the inner-shell transitions, i.e., one  $1s$  electron being excited to the  $2p$  orbital. These  $K$ -shell excited states are well above the single-electron ionization threshold, and the autoionization widths generally exceed the Doppler and Stark widths for most  $K$ -shell transitions from the low-lying states of different Al ionization stages. Therefore the autoionization width has a large effect on the radiative opacity or transmission. Secondly, in the range  $h\nu \lesssim 1$  keV, accurate photoionization cross sections, especially detailed treatments of the resonances, are required to reproduce the structures experimentally observed. Our photoionization cross sections were obtained by using the close-coupling scheme implemented by  $R$ -matrix codes [28]. The  $R$ -matrix method is quite effective in treating the autoionization resonances, as demonstrated by our previous work [29–31]. In spite of the experimental and theoretical studies mentioned above, there is still a lack of complete understanding of the radiative opacity of plasmas. The purpose of the present paper is to carry out a systematic study of the opacity of aluminum plasmas with varieties of density and temperature. Particular attention is given to the influence of the detailed treatment of spectral lines on the Rosseland mean opacity under different thermodynamical conditions. After a brief introduction of the method of calculation (Sec. II), we present our theoretical results in Sec. III. In Sec. III A, we give an overview of our calculated opacity and transmission in the photon energy range of 70–250 eV for the aluminum plasma at a temperature of 20 eV and a density of 0.01 g/cm<sup>3</sup>. The transmission in this energy interval has been experimentally measured by Winhart *et al.* [15,16]. Analyses were made to clarify the difference between the opacities and transmissions obtained by the DTA and average atom (AA) models. Then in Sec. III B we obtain the spectrally resolved opacities and Rosseland and Planck mean opacities of the aluminum plasma of a 40 eV isothermal sequence, with densities vary from 0.0001 to 0.64 g/cm<sup>3</sup>. In Secs. III C and III D, similar calculations are carried out for a 0.01 g/cm<sup>3</sup> isodense sequence, with temperatures varying from 15 eV to 60 eV, and for a sequence with average ionization degree  $Z^* \sim 7.13$ , with the densities of 0.0001, 0.001, 0.01, and 0.1 g/cm<sup>3</sup>. In Sec. III E, we check the sensitivities of the Rosseland mean opacity to the accuracy of the linewidth caused by the electron impact broadening mechanism by artificially reducing its width by 50% or increasing it twice. All of the calculations were carried out in the range  $h\nu \lesssim 1$  keV. It is this spectral range that determines the Rosseland and Planck mean opacities under these plasma conditions. The calculations are carried out using the DTA and average atom models to have a comparison between the two results. By presenting the three sequences, we expect that we will have a relatively complete understanding of the opacities of aluminum plasmas over a relatively wide temperature and density range. Finally, the conclusions are presented in Sec. III F.

## II. METHOD OF CALCULATION

The details of DTA calculations of opacities have been given elsewhere [26,27,32]. The theoretical details for the computation of photoionization cross sections in the close-

coupling approximation employing the  $R$ -matrix method have also been given in our previous papers [29–31]. Here only a brief description is presented. For a LTE plasma, the radiative opacity at radiation of energy  $h\nu$  for a plasma of mass density  $\rho$  and temperature  $T$  is given by

$$\rho\kappa'(h\nu) = \sum_i \left[ \left( \sum_{it'} N_{it'} \sigma_{it'}(h\nu) + \sum_t N_{it} \sigma_{it}(h\nu) \right) + \mu_{iff}(h\nu) \right] (1 - e^{-h\nu/kT}) + \mu_{scatt}(h\nu), \quad (1)$$

where  $\kappa'(h\nu)$  is the total opacity, the prime on the opacity denotes that stimulated emission has been included in the calculation,  $\sigma_{it'}(h\nu)$  is the cross section for photoexcitation from term  $t$  to  $t'$  of ion  $i$ ,  $\sigma_{it}(h\nu)$  is the photoionization cross section from term  $t$  of ion  $i$ , and  $\mu_{iff}(h\nu)$  and  $\mu_{scatt}(h\nu)$  are the absorption coefficients contributed by free-free absorption and scattering, respectively.  $N_{it}$  is the population density for term  $t$  of ion stage  $i$  obtained from the Boltzmann distribution function

$$N_{it} = g_{it} (N_i / Z_i) e^{-E_{it}/kT}, \quad (2)$$

where  $g_{it}$  is the statistical weight for term  $t$  of ion  $i$ ,  $Z_i$  is the partition function of ion  $i$ ,  $N_i$  is the population of ion  $i$ ,  $E_{it}$  is the energy of term  $t$  of ion  $i$  above the ground state, and  $k$  is the Boltzmann constant.  $N_i$  can be obtained by solving the Saha equation [26,33]. The continuum lowering is considered by using the Debye-Hückel model [34]. The bound-bound cross section for a given line may be expressed in terms of the oscillator strength  $f_{it'}$  as

$$\sigma_{it'} = \frac{\pi h e^2}{m_e c} f_{it'} S(h\nu), \quad (3)$$

where  $S$  is the line shape function,  $h$  Planck's constant,  $c$  the speed of light in vacuum,  $e$  the electron charge, and  $m_e$  the electron rest mass. In the present work,  $S$  is taken to be the Voigt profile which takes account of both the Doppler and Stark broadening. The expression for the Voigt profile and the determinations of the Doppler and Stark widths can be found in our previous paper [27].

The calculation of the Stark broadening is complicated and even the semiclassical method needs elaborate considerations. The available data for the Stark widths are not sufficient for the opacity calculations. The requirement for the rapid calculation of spectral linewidths has led to the development of a number of approximate methods [3,35–38]. Most of these methods are simplified semiclassical or semiempirical ones. Seaton [39] adopted a method of rapid calculation of the Stark widths based on quantum mechanical calculations. In the present paper, the Stark widths (in eV) were obtained from the simplified semiempirical method [37]

$$\Gamma_l = N_e \frac{8\pi}{6} \frac{\hbar^3}{m^2 e} \left( \frac{2m}{\pi kT} \right)^{1/2} \frac{\pi}{\sqrt{3}} \left( 0.9 - \frac{1.1}{z} \right) \times \sum_{j=i,f} \left( \frac{3n_j}{2z} \right)^2 (n_j^2 - l_j^2 - l_j - 1), \quad (4)$$

where  $n_i(l_i)$  and  $n_f(l_f)$  are the effective principal (orbital angular momentum) quantum numbers of the lower and upper energy levels of the transition, respectively.

The fraction of radiation transmitted  $F$  at energy  $h\nu$  with respect to some incident source of arbitrary intensity is given by

$$F(h\nu) = e^{-\rho\kappa'(h\nu)L}, \quad (5)$$

where  $L$  is the path length traversed by the light source through the plasma. The function  $F$  is integrated over a Gaussian function, with the full width corresponding to the spectrometer resolution, to obtain the final transmission spectrum, which can be compared directly with the experiment.

In practical applications, such as radiative transfer through hot dense plasmas, Rosseland and Planck mean opacities are required. These two mean opacities are defined by

$$\frac{1}{K_R} = \int_0^\infty \frac{W_R(u) du}{\kappa'(u)}, \quad (6)$$

and

$$K_P = \int_0^\infty [\kappa'(u) - \kappa_{scatt}] W_P(u) du, \quad (7)$$

where  $u = h\nu/kT$ ,  $\kappa_{scatt}$  is the absorption coefficient contributed by scattering, and  $W_R$  and  $W_P$  are the Rosseland and Planck weighting functions, respectively, given by

$$W_R(u) = \frac{15}{4\pi^4} \frac{u^4 \exp(-u)}{[1 - \exp(-u)]^2} \quad (8)$$

and

$$W_P(u) = \frac{15}{\pi^4} \frac{u^3 \exp(-u)}{1 - \exp(-u)}. \quad (9)$$

The method of calculation using the AA model can be found elsewhere [40–42]; no detailed description will be given here. In the present AA model, the one-electron orbital energies are obtained by solving the radial Schrödinger equation with a definite boundary self-consistently. The radial boundary, i.e., the size of the atom, is determined by the density of the plasma. The fractional occupation numbers at each one-electron orbital obey Fermi-Dirac distribution. Due to the restriction of the limited size of the atom, some of the orbitals, which are bound states for the free atoms, become ionized states. The ionization of an orbital is also temperature dependent, because the average ionization degree has

influence on the self-consistent potential. Therefore, the so-called continuum lowering has been considered quite differently in our DTA and AA calculations. The width of the bound-bound transitions in this AA model is calculated by considering the fluctuations of the occupation numbers according to the suggestion of Rose [18]. Because the one-electron transitions in the AA model are not distinguished for different ions and different terms of the same ion, the shape and width calculated by the method of Rose [18] represent the shape and width of the so-called unresolved transition array. The individual spectral lines are completely unresolved in the AA model results. These kinds of statistical treatment are only reasonable when the real transition lines are merged completely due to Stark or Doppler broadening. Only aluminum plasmas in LTE are considered in this paper. The two kinds of calculation, the DTA model and the AA model, are carried out independently without any artificial attempt to assure that they are consistent with each other, although physically some of the quantities, for example, the average ionization degree, predicted by them should be so.

### III. RESULTS AND DISCUSSION

#### A. Opacity and transmission at 20 eV and 0.01 g/cm<sup>3</sup>

The details of the results at this density and temperature have been reported in our previous paper [27]. We will not repeat the main parts of the previous paper, but a short description will be given for the convenience of the reader to access the accuracy of our calculation by comparing the spectrally resolved transmission in a relatively low-energy region of the photon, which was measured by Winhart *et al.* [15,16]. For this case, the average ionization degree is 4.2, which is obtained by solving the Saha equation, in good agreement with the theoretical result of 4.3 obtained by the OPAL code [17]. Among the various ionization stages, Al V ions are the most abundant, accounting for 50% of the total particle population, and the next ones are Al VI and Al IV ions, accounting for 32% and 16%, respectively.

Figure 1 shows the radiative opacities and the corresponding transmissions in the photon energy range of 70–250 eV, corresponding to the region experimentally observed [15,16]. In Fig. 1, the solid line refers to the results obtained by the DTA approximation, the dashed line to the results obtained by the AA model. In Fig. 1(b), the long dashed line refers to the experimental spectrum [15,16]. In order to have optimum coincidence with the experimental spectrum, our DTA results have been shifted to lower photon energy by 2.6 eV. Detailed discussions of the structures and comparisons between our DTA results and the experiment can be found in our previous paper, but one can find general good agreement between the calculated transmission spectra by our DTA model and the measurement by Winhart *et al.* [15,16]. According to Eqs. (6)–(9), the spectral resolved opacity in this energy region contributes the main part of the Rosseland and Planck mean opacities. The AA model, for which the results are also displayed in Fig. 1, gives very poor agreement with the measured spectra.

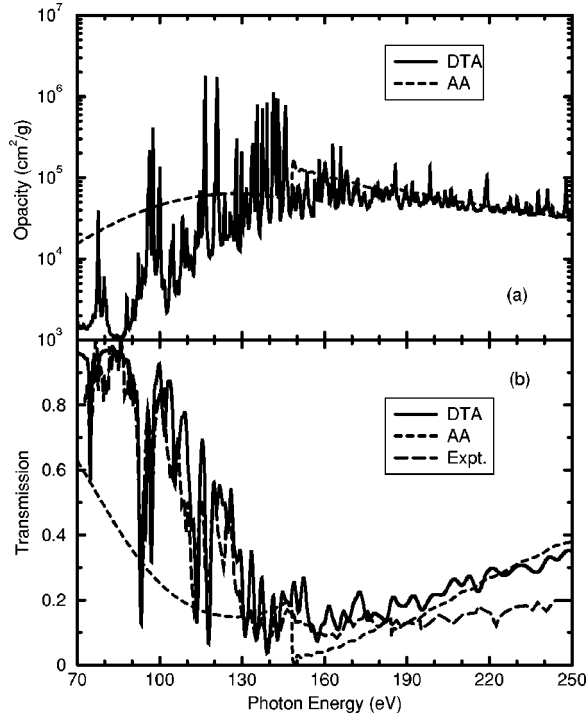


FIG. 1. (a) The spectrally resolved radiative opacity and (b) transmission for an aluminum plasma at a temperature of 20 eV and a density of 0.01 g/cm<sup>3</sup>. In (b), the DTA transmission has been convolved with the reported spectrometer resolution. Note that the spectrometer resolution varies with photon energy.

**B. Opacities of the 40 eV isothermal sequence**

The differences between the spectrally resolved and mean opacities under the above typical experimental condition [15,16] obtained by the DTA and AA models are due to two main sources. The first one is the energy shift of the absorption peaks of the AA model relative to the true positions. The second one is the smoothing of the fine line structures made artificially in the AA model. As defined by Eqs. (7) and (9), the Planck mean opacity is a linear weighted average, while the Rosseland mean opacity is a harmonic weighted average. Therefore, the unphysical energy shift of the absorption peaks of the AA model induces errors in both the Rosseland and Planck means, while the smoothing over the detailed lines in the AA model changes mainly the Rosseland mean opacity. The question is when both, one, or even neither of these two factors are significant enough to cause unacceptable errors. To have an overall view of the question, we have made a systematic study of the spectrally resolved and Rosseland and Planck mean opacities under different plasma conditions for three sequences: a 40 eV isothermal one, a 0.01 g/cm<sup>3</sup> isodense one, and one of average ionization degree  $Z^* \sim 7.13$ .

First, as an example of an isothermal sequence, we calculated the radiative opacities of aluminum plasmas at a temperature of 40 eV and mass densities range from 0.0001 to 0.64 g/cm<sup>3</sup>. The spectrally resolved opacities and Rosseland and Planck mean opacities at 16 sample points of density, which are listed in Table I, are calculated by both the DTA and AA models. Because there are too many data, it is im-

TABLE I. The Rosseland and Planck mean opacities obtained by our DTA and AA models at a temperature of 40 eV and different densities (in g/cm<sup>3</sup>).

Density (g/cm <sup>3</sup> )	DTA Rosseland	DTA Planck	AA Rosseland	AA Planck
0.0001	68	4236	376	4810
0.0002	156	5992	707	6422
0.0004	316	8130	1277	8310
0.0008	644	10481	2220	10468
0.001	845	11380	2620	11210
0.002	1698	13710	4343	13718
0.004	3435	15900	6763	16425
0.008	6305	18636	9908	19301
0.01	7328	19576	11067	20280
0.02	10900	22966	14698	23352
0.04	14673	26802	18151	26517
0.08	17409	30305	21105	29973
0.1	17821	31064	21919	30957
0.16	19216	33645	23781	33960
0.32	19879	37166	25055	37223
0.64	20805	42423	27093	43835

practical to give all these data in the present paper. A part of them, Figs. 2(a)–2(d) show the spectrally resolved radiative opacities at densities of 0.0001, 0.001, 0.01, and 0.1 g/cm<sup>3</sup>, respectively. The solid lines refer to the DTA opacities and the gray lines to the AA opacities. One can see from Figs. 2(a)–2(b) that at densities of 0.0001 and 0.001 g/cm<sup>3</sup> the widths of the spectral lines are too small to coalesce to fill in the gaps between the discrete lines. As a matter of fact, the Stark and Doppler widths are indeed small and they compete with each other for different transitions of plasmas at the density of 0.001 g/cm<sup>3</sup>.

To have a quantitative understanding, we turn to the line-widths caused by the two kinds of broadening mechanism. For aluminum plasma at a temperature of 40 eV and a density of 0.001 g/cm<sup>3</sup>, Al x ions are the most abundant, representing 42% of the total particle population, according to our calculation. For a transition of  $2p-3d$  from the ground state of Al x, the Stark width can be calculated to be 2 meV from Eq. (4) and the Doppler width is 10 meV. The Doppler width is four times larger than Stark width. While for a transition of  $2s-2p$  from the ground state of Al x, the Stark width is 1 meV and the Doppler width is 0.8 meV. In this case, the Doppler width is a little smaller than the Stark width. One can imagine that the Doppler broadening will dominate gradually as the density of the plasma decreases. When the density is decreased by 10 times, i.e., 0.0001 g/cm<sup>3</sup>, the Doppler broadening is the main broadening mechanism. On the other hand, when the density is increased by 10 times, i.e., 0.01 g/cm<sup>3</sup>, the Doppler widths are basically the same as those at 0.001 g/cm<sup>3</sup> density, but the Stark widths increase greatly because the electron density increases considerably. From the inspection of Fig. 2(c), one can see that, although there is still nonoverlapping between some lines, some other lines begin to coalesce to fill the gaps. When the

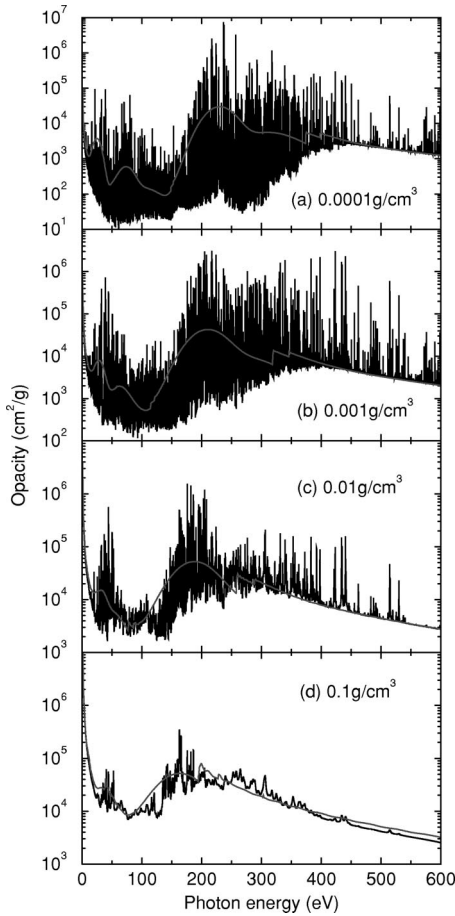


FIG. 2. The spectrally resolved radiative opacities for aluminum plasmas at a temperature of 40 eV and densities of (a) 0.0001, (b) 0.001, (c) 0.01, and (d) 0.1 g/cm<sup>3</sup>. The solid lines refer to the DTA results and the grey lines to the AA results.

density is increased further to 0.1 g/cm<sup>3</sup>, the Stark width becomes so large that all the absorption lines overlap greatly. They have merged into a much smoother curve. At this density, the Stark broadening dominates over Doppler broadening. The spectrally resolved opacities obtained by our DTA model become closer and closer to those obtained by the AA model with increasing density. From these analyses, one can conclude that the differences between the Rosseland mean opacities obtained by the two models become larger and larger as the mass densities get lower and lower. On the contrary, with increasing density, the agreement between the Rosseland and Planck mean opacities by the two models will become closer and closer. The final results are indeed so, and such a conclusion can easily be seen from Fig. 3, which shows the variations of the Rosseland and Planck mean opacities as a function of the density. The mean opacities at the 16 sample points of density are also given in Table I.

From Table I and Fig. 3, one can see that the agreement between the Planck mean opacities obtained by the DTA and AA models is better than that of the Rosseland mean opacities. The relative difference between the DTA and AA Planck mean opacities is less than 14%. It is 13.6% at a density of 0.0001 g/cm<sup>3</sup> and decreases to 1.5%, 3.6%, and 0.34% at densities of 0.001, 0.01, and 0.1 g/cm<sup>3</sup>, respectively. As

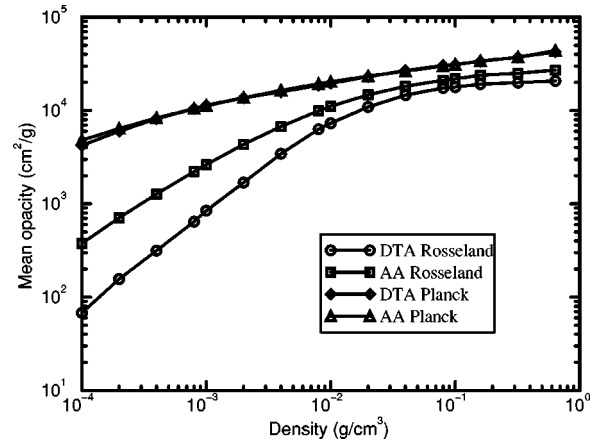


FIG. 3. The Rosseland and Planck mean opacities for aluminum plasmas as a function of density at a temperature of 40 eV.

mentioned above, as the Planck mean opacity is a weighted linear average over the spectrally resolved opacities, only an energy shift of the absorption peaks causes considerable change to the average values. In Fig. 1, it was shown that, although the position of the main absorption peak around 200 eV varies slightly with the density, the positions predicted by the DTA and AA models agree well with each other over the whole range of density. This is not always true for any density and temperature, although it seems that considerable discrepancies have only been found below 30 eV. Because the Rosseland mean is a weighted integration over the inverse of the spectrally resolved opacity, the result is much more influenced by the smoothed absorption structures in the AA model. From Fig. 3, one can see that the agreement between the Rosseland mean opacities obtained by our DTA and AA models becomes better and better as the density increases. For densities above 0.01 g/cm<sup>3</sup>, the difference between the DTA and AA Rosseland mean opacities is no more than 40%. This conclusion is also temperature dependent. Both the Rosseland and Planck mean opacities increase monotonically with density over the 0.0001–0.64 g/cm<sup>3</sup> range, for either the DTA or AA model. Application of the Saha equation, with a simple continuum lowering, at a density like 0.64 g/cm<sup>3</sup> is certainly questionable. By comparing with the AA model, we find that the highest occupied orbitals predicted by the two models are the same for the highest densities we studied here.

### C. Opacities of the 0.01 g/cm<sup>3</sup> isodense sequence

Next, we turn to the opacities at a density of 0.01 g/cm<sup>3</sup> and temperatures from 15 to 60 eV. As part of them, Figs. 4(a)–4(d) shows the spectrally resolved opacities at temperatures of 20, 30, 50, and 60 eV, respectively. From the inspection of Fig. 4, one can see that the spectral line shapes and widths do not differ considerably at different temperatures, but the maximal value of the opacities shifts toward higher photon energy as the temperature increases. The latter conclusion can be easily understood because the average ionization degree of the plasma increases as the plasma temperature increases. The increase of the average ionization degree means that the most abundant ions in the plasma shift to

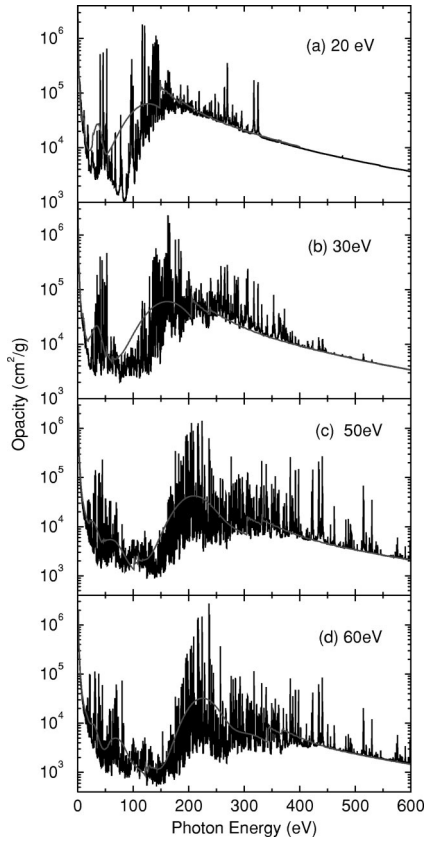


FIG. 4. The spectrally resolved radiative opacities for aluminum plasmas at a density of  $0.01 \text{ g/cm}^3$  and temperatures of (a) 20, (b) 30, (c) 50, and (d) 60 eV.

higher ionization stages. For the same type of transition from different ionization stages, for example,  $2p-3s$ , the transition energies of the higher ionization stages are usually larger than those of lower ionization stages. Therefore, the maximal value of the opacities shifts toward higher photon energy as the temperature increases. The former conclusion cannot be seen as directly as the latter. As discussed in Sec. III A, the Stark broadening is the main broadening mechanism at the density of  $0.01 \text{ g/cm}^3$ . From the semiempirical expression for the Stark width [Eq. (4)], we know that the Stark width increases with electron density, and decreases with increasing ionic charge. With the increase of temperature and density unchanged, the average ionization degree increases. As a result, the electron density and ionic charge of the most populated species will increase at higher temperatures. The competition between the two factors results in the closeness of the linewidths for isodense sequence. The positions of the main absorption peaks around 200 eV predicted by the DTA and AA models generally coincide well at temperatures above 30 eV. As expected, the Planck mean opacities of the two models for these temperatures do not differ very much.

Table II gives the Rosseland and Planck mean opacities for this isodense sequence. Figure 5 shows the variations of the two means with temperature. From Table II and Fig. 5, one can see that the variation of the two mean opacities with temperature is more complicated than with density. The Planck mean opacities obtained by our DTA and AA models

TABLE II. The Rosseland and Planck mean opacities obtained by our DTA and AA models at a density of  $0.01 \text{ g/cm}^3$  and different temperatures (in eV).

$T$ (eV)	DTA Rosseland	DTA Planck	AA Rosseland	AA Planck
20	4184	24891	22520	30402
22	4650	23795	22363	29354
25	5608	24336	20866	29354
30	7734	25223	17430	26572
35	8520	22963	14140	23576
40	7328	19576	11067	20280
45	5565	17225	8455	17110
50	4508	15215	6374	14165
55	3582	12585	4781	11489
60	2709	9785	3505	9071

have larger differences at temperatures below 30 eV (the maximum of which is 23.6% at 22 eV) than at temperatures above 30 eV (the maximum is 8.7% at 55 eV). Both our DTA and AA models show a shoulder at a temperature of about 25 eV. At about 45 eV, the Planck mean opacities from the DTA and AA models are equal to each other. For the Rosseland mean opacities, both models predict a similar trend in the temperature range of 15–60 eV. They increase with temperature at first and then decrease, but the temperature of the turning point is different. The DTA model predicts a maximum Rosseland mean at about 35 eV, while the corresponding AA model at about 20 eV. The difference in the Rosseland mean between the two models is caused by the different treatment of the bound-bound and bound-free absorption processes. At the temperature of 20 eV, the AA Rosseland mean is 4.38 times larger than the corresponding DTA value. With an increase of temperature, the differences begin to decrease. At the temperature of 35 eV, the AA Rosseland mean is only 66% larger than the corresponding DTA value. Above 35 eV, the differences become even more smaller. At 60 eV, the relative difference between the two models is only 29%.

#### D. Opacities of the $Z^* \sim 7.13$ sequence

Under the plasma condition of 40 eV temperature and  $0.01 \text{ g/cm}^3$  density, the average ionization degree  $Z^*$  is

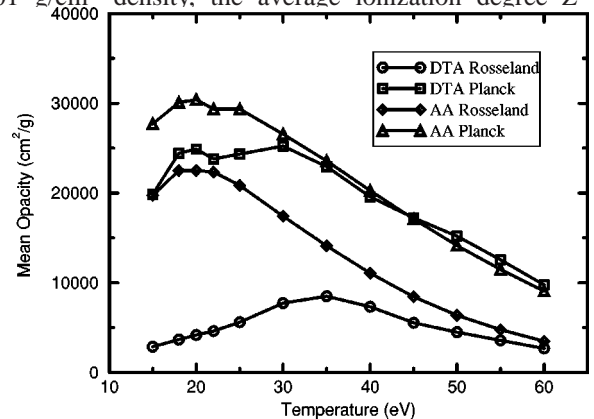


FIG. 5. The Rosseland and Planck mean opacities for aluminum plasmas as a function of temperature at a density of  $0.01 \text{ g/cm}^3$ .

TABLE III. Integer charge state distribution of an aluminum plasma ( $T=40$  eV,  $\rho=0.0135$  g/cm<sup>3</sup>). For comparison, our results obtained by solving the Saha equation and those of Faussurier *et al.* [43] are given.

Charge state	Present work	Faussurier <i>et al.</i> [43]
Al VI	3.85%	2.65%
Al VII	24.84%	22.33%
Al VIII	45.62%	46.95%
Al IX	22.72%	24.65%
Al X	2.64%	3.23%

7.13, obtained by solving the Saha ionization equilibrium equation. This result should be correct and reliable when we compare our other results for the Saha equation with other theoretical ones. Faussurier *et al.* [43] proposed a method for accounting for the various ionization stages of a LTE plasma based on the AA model. The method can also be used to estimate the integer charge state distribution in the plasma. For an aluminum plasma at a temperature of 40 eV and a mass density of 0.0135 g/cm<sup>3</sup>, they calculated the average ionization degree to be  $Z^*=7.036$ . Considering the lower density 0.01 g/cm<sup>3</sup> rather than 0.0135 g/cm<sup>3</sup> in our case, our value of the average ionization degree  $Z^*=7.13$  seems natural. The value 7.13 is a little larger than 7.036 because the density of 0.01 g/cm<sup>3</sup> is less than 0.0135 g/cm<sup>3</sup>. As a matter of fact, we have also solved the Saha equation for the aluminum plasma at a temperature of 40 eV and a density of 0.0135 g/cm<sup>3</sup>. According to our calculation, the average ionization degree is 6.95, which is rather close to the value 7.036 obtained by Faussurier *et al.* [43]. Nevertheless, as Faussurier *et al.* pointed out that their method predicted an ionization higher than other theoretical results obtained by Kilcrease *et al.* [22]; thus our ionization degree of 6.95 agrees better with that obtained by Kilcrease *et al.* They obtained their results also by solving the Saha equation, but the necessary atomic data for the calculations of the partition functions were obtained from the unresolved transition arrays approximation [44]. Therefore, we are confident that our results obtained from solving the Saha equation are correct and reliable. In Table III, the ion fractions for the LTE aluminum plasma at  $T=40$  eV and  $\rho=0.0135$  g/cm<sup>3</sup> are given. For comparison, both our results and those obtained by Faussurier *et al.* [43] are given. Both results predict similar distributions and only three main ion species exist in the plasma.

For the  $Z^*\sim 7.13$  sequence, we have considered another three cases: 25.24 eV and 0.0001 g/cm<sup>3</sup>, 31.04 eV and 0.001 g/cm<sup>3</sup>, and 53.35 eV and 0.1 g/cm<sup>3</sup>. Figure 6 shows the spectrally resolved opacities of this  $Z^*\sim 7.13$  sequence. The corresponding Rosseland and Planck mean opacities are given in Table IV. They are plotted in Fig. 7 as a function of the density. The different temperatures for this sequence are shown at the top of the corresponding results. Similar conclusions to those noted for in Fig. 2 can be drawn from a comparison of the spectrally resolved opacities, although the temperatures are different for the present cases.

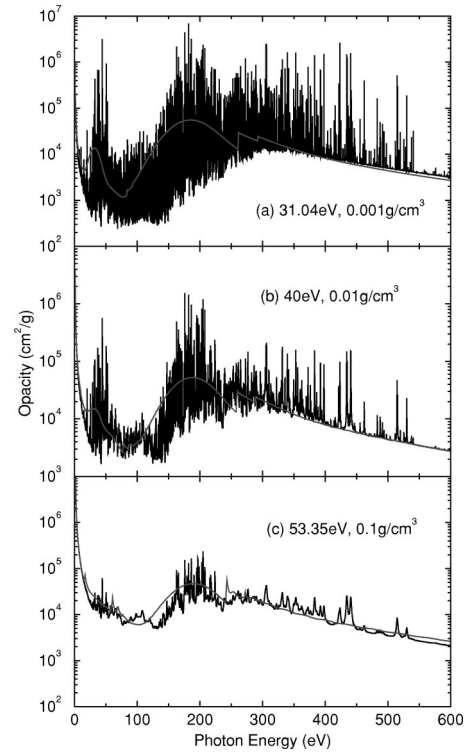


FIG. 6. The spectrally resolved radiative opacities for aluminum plasmas of the  $Z^*\sim 7.13$  sequence: (a) 31.04 eV and 0.001 g/cm<sup>3</sup>, (b) 40 eV and 0.01 g/cm<sup>3</sup>, and (c) 53.35 eV and 0.1 g/cm<sup>3</sup>.

#### E. Sensitivities of the Rosseland mean opacity on the accuracy of the linewidth

For low-density plasmas, the true structure of the spectral lines has to be treated carefully in order to get correct results for both the transmission spectra and the Rosseland mean opacity. The linewidth plays an important role in these kinds of calculation. Accurate determination of the linewidth is a complicated task and a variety of approximations have to be involved in various models. Therefore, the sensitivity of the Rosseland mean opacity to the linewidth would provide helpful information to judge the reliability of the results.

In the present study, the line broadening due to electron impact is calculated by using a semiempirical formula given by Eq. (4), while the collision between the ions has not been considered explicitly. Generally it is believed that the line broadenings by electron impact and ion collision are similar. From our calculations, it has been shown that the semiempirical formula of Eq. (4) gives results quite close to those of a

TABLE IV. The Rosseland and Planck mean opacities obtained by our DTA and AA models for  $Z^*\sim 7.13$  sequence.

$T$ (eV)	$\rho$ (g/cm <sup>3</sup> )	DTA Rosseland	DTA Planck	AA Rosseland	AA Planck
25.24	0.0001	258	10153	2309	11664
31.04	0.001	1335	14318	5282	16193
40	0.01	7328	19576	11067	20280
53.35	0.1	11664	22145	12157	22134

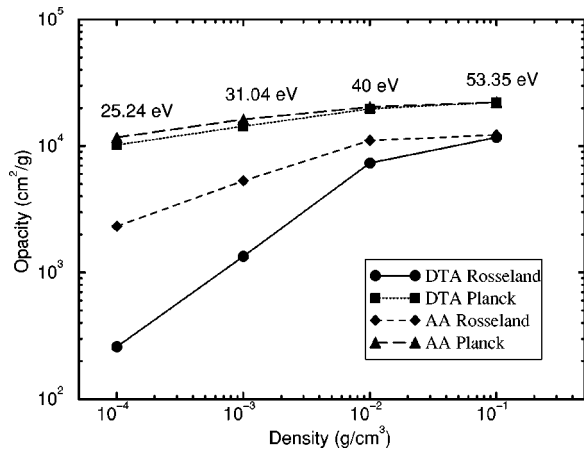


FIG. 7. The Rosseland and Planck mean opacities for aluminum plasmas of the  $Z^* \sim 7.13$  sequence as a function of density at different temperatures.

quantum mechanical calculation [45]. By comparing with limited experimental data, the accuracy of this kind of treatment was estimated to be about 50%. In the present case, the dependence of the Rosseland mean opacity on the linewidth was shown just by artificially reducing the linewidth given by Eq. (4) by 50% or increasing it twice. The results at a few typical densities and temperatures are collected in Table V. One can see that at 40 eV and  $0.004 \text{ g/cm}^3$  the Rosseland mean opacity changes no more than 15%, while at 40 eV and  $0.1 \text{ g/cm}^3$  it changes even less than 5%. The results are quite encouraging, as these densities and temperatures are often found in practical applications.

**F. Conclusion**

In summary, a systematic study of the spectrally resolved and Rosseland and Planck mean radiative opacities of aluminum plasmas have been carried out by two different methods: the detailed-term-accounting approximation and the average atom model. Results are presented for a 40 eV isothermal sequence, a  $0.01 \text{ g/cm}^3$  isodense sequence, and a

TABLE V. Changes of the Rosseland mean opacity at 40 eV by reducing and increasing individual linewidth artificially. Case B corresponds to the results with electron impact broadening using Eq. (4). Cases A and C correspond to the results obtained by artificially reducing the linewidth given by Eq. (4) by 50% and increasing it twice, respectively.

Plasma condition	Difference		Difference	
	A	(%)	B	C
40 eV, $0.004 \text{ g/cm}^3$	2992	12.8%	3435	3892
40 eV, $0.01 \text{ g/cm}^3$	6565	10.4%	7328	8024
40 eV, $0.04 \text{ g/cm}^3$	13690	6.7%	14673	15468
40 eV, $0.1 \text{ g/cm}^3$	17051	4.3%	17821	18489

sequence of average ionization degree  $Z^* \sim 7.13$ . For most densities and temperatures presented here, the distribution range and position of the transition array predicted by the AA model have no significant discrepancies from those of the DTA model, resulting in Planck mean opacities with small differences. However, these findings cannot be assured for any density, temperature, or material. The present results also show that the differences between the Rosseland and Planck mean opacities obtained by the DTA and AA models are mainly due to the energy shift of the absorption peaks and the smoothing of the individual lines made in the AA model. The uncertainty of the opacities of the DTA model due to the limited accuracy of the individual spectral linewidths has been shown to be acceptable for plasma densities above a critical value.

**ACKNOWLEDGMENTS**

This work was supported by the National Science Fund for Distinguished Young Scholars under Grant No. 10025416, the National Natural Science Foundation of China under Grant No. 19974075, the National High-Tech ICF Committee in China, and the China Research Association of Atomic and Molecular Data.

[1] M. J. Seaton, *J. Phys. B* **20**, 6363 (1987).  
 [2] K. A. Berrington, P. G. Burke, K. Butler, M. J. Seaton, P. J. Storey, K. T. Taylor, and Yu Yan, *J. Phys. B* **20**, 6379 (1987).  
 [3] The Opacity Project, *The Opacity Project* (Institute of Physics Publishing, Bristol, 1995), Vols. 1 and 2.  
 [4] D. G. Hummer, K. A. Berrington, W. Eissner, A. K. Pradhan, H. E. Saraph, and J. A. Tully, *Astron. Astrophys.* **279**, 298 (1993).  
 [5] S. J. Davidson, J. M. Foster, C. C. Smith, K. A. Warburton, and S. J. Rose, *Appl. Phys. Lett.* **52**, 847 (1988).  
 [6] S. J. Davidson, C. L. S. Lewis, D. O'Neill, S. J. Rose, J. M. Foster, and C. C. Smith, in *Laser Interaction with Matter*, edited by G. Velarde, E. Minguez, and J. M. Perlado (World Scientific, Singapore, 1989).  
 [7] T. S. Perry, S. J. Davidson, F. J. D. Serduke, D. R. Bach, C. C. Smith, J. M. Foster, R. J. Doyas, R. A. Ward, C. A. Iglesias, F. J. Rogers, J. Abdallah, Jr., R. E. Stewart, J. D. Kilkenney, and R. W. Lee, *Phys. Rev. Lett.* **67**, 3784 (1991).  
 [8] C. A. Iglesias, M. H. Chen, D. L. McWilliams, J. K. Nash, and F. J. Rogers, *J. Quant. Spectrosc. Radiat. Transf.* **54**, 185 (1995).  
 [9] L. Aschke, S. Depierreux, K. G. Estabrook, K. B. Fournier, J. Fuches, S. Glenzer, R. W. Lee, W. Rozmus, R. S. Thoe, and P. E. Young, *J. Quant. Spectrosc. Radiat. Transf.* **65**, 23 (2000).  
 [10] C. Chenais-Popovics, F. Gilleron, M. Fajardo, H. Merdji, T. MiBalla, J. C. Gauthier, P. Renaudin, S. Gary, J. Bruneau, F. Perrot, T. Blenski, W. Fölsner, and K. Eidmann, *J. Quant. Spectrosc. Radiat. Transf.* **65**, 117 (2000).  
 [11] U. Andiel, K. Eidmann, and K. Witte, *Phys. Rev. E* **63**, 026407 (2001).  
 [12] T. S. Perry, R. I. Klein, D. R. Bach, K. S. Budil, R. Cauble, H. N. Kornblum, Jr., R. J. Wallace, and R. W. Lee, *Phys. Rev. E*

- 58**, 3739 (1998).
- [13] K. G. Whitney, J. W. Thornhill, P. E. Pulsifer, J. P. Apruzese, T. W. L. Sanford, T. J. Nash, R. C. Mock, and R. B. Spielman, *Phys. Rev. E* **56**, 3540 (1997).
- [14] C. Y. Côté, J. C. Kieffer, and O. Peyrusse, *Phys. Rev. E* **56**, 992 (1997).
- [15] G. Winhart, K. Eidmann, C. A. Iglesias, A. Bar-Shalom, E. Minguez, A. Rickert, and S. J. Rose, *J. Quant. Spectrosc. Radiat. Transf.* **54**, 437 (1995).
- [16] G. Winhart, K. Eidmann, C. A. Iglesias, and A. Bar-Shalom, *Phys. Rev. E* **53**, R1332 (1996).
- [17] F. J. Rogers and C. A. Iglesias, *Astrophys. J., Suppl. Ser.* **79**, 507 (1992).
- [18] S. J. Rose, *J. Phys. B* **25**, 1667 (1992).
- [19] E. Mínguez, J. F. Serrano, and M. L. Gámez, *Laser Particle Beams* **6**, 265 (1988).
- [20] A. Bar-Shalom, J. Oreg, W. H. Goldstein, D. Shvarts, and A. Zigler, *Phys. Rev. A* **40**, 3183 (1989).
- [21] A. Bar-Shalom, J. Oreg, and W. H. Goldstein, *J. Quant. Spectrosc. Radiat. Transf.* **51**, 27 (1994).
- [22] D. P. Kilcrease, J. Abdallah, Jr., J. J. Keady, and R. E. H. Clark, *J. Phys. B* **26**, L717 (1993).
- [23] J. Abdallah, Jr. and R. E. H. Clark, *J. Appl. Phys.* **69**, 23 (1991).
- [24] C. A. Iglesias, J. K. Nash, M. H. Chen, and F. J. Rogers, *J. Quant. Spectrosc. Radiat. Transf.* **51**, 125 (1994).
- [25] A. Rickert, *J. Quant. Spectrosc. Radiat. Transf.* **54**, 325 (1995); S. J. Rose, *ibid.* **51**, 317 (1994).
- [26] Jiaolong Zeng, Fengtao Jin, Jianmin Yuan, Qisheng Lu, and Yongsheng Sun, *Phys. Rev. E* **62**, 7251 (2000).
- [27] Jiaolong Zeng, Jianmin Yuan, and Qisheng Lu, *Phys. Rev. E* **64**, 066412 (2001).
- [28] K. A. Berrington, W. B. Essner, and P. H. Norrington, *Comput. Phys. Commun.* **92**, 290 (1995).
- [29] Jiaolong Zeng, Jianmin Yuan, Zengxiu Zhao, and Qisheng Lu, *Eur. Phys. J. D* **11**, 167 (2000).
- [30] Jiaolong Zeng, Jianmin Yuan, and Qisheng Lu, *Phys. Rev. A* **62**, 022713 (2000); **64**, 042704 (2001).
- [31] Jiaolong Zeng, Jianmin Yuan, and Qisheng Lu, *J. Phys. B* **34**, 2823 (2001).
- [32] Jiaolong Zeng, Fengtao Jin, and Jianmin Yuan, *Chin. Phys. Lett.* **18**, 924 (2001).
- [33] R. D. Cowan, *The Theory of Atomic Structure and Spectra* (University of California Press, Berkeley, CA, 1981).
- [34] D. J. Heading, J. S. Wark, G. R. Bennett, and R. W. Lee, *J. Quant. Spectrosc. Radiat. Transf.* **54**, 167 (1995), and references therein.
- [35] H. R. Griem, *Spectra Line Broadening by Plasma* (Academic Press, New York, 1974).
- [36] M. S. Dimitrijevic and N. Konjevic, *J. Quant. Spectrosc. Radiat. Transf.* **24**, 451 (1980).
- [37] M. S. Dimitrijevic and N. Konjevic, *Astron. Astrophys.* **172**, 345 (1987).
- [38] M. S. Dimitrijevic and N. Konjevic, in *Spectral Line Shapes 9*, edited by B. Wende (de Gruyter, Berlin, 1981), pp. 211–239.
- [39] M. J. Seaton, *J. Phys. B* **20**, 6431 (1987); **22**, 3603 (1989); **23**, 3255 (1990).
- [40] H. Mayer, Los Alamos Scientific Report No. LA-647, 1947 (unpublished).
- [41] J. M. Green, *J. Quant. Spectrosc. Radiat. Transf.* **4**, 639 (1964).
- [42] B. F. Rozsnyai, *Phys. Rev. A* **5**, 1137 (1972).
- [43] G. Faussurier, C. Blancard, and A. Decoster, *Phys. Rev. E* **56**, 3474 (1997).
- [44] J. Bauche, C. Bauche-Arnoult, and M. Klapisch, *Adv. At. Mol. Phys.* **23**, 131 (1987).
- [45] Jiaolong Zeng, Jianmin Yuan, Zengxiu Zhao, and Qisheng Lu, *High Power Laser Particle Beams* **13**, 60 (2001) (in Chinese); Jiaolong Zeng, Qingping Yuan, and Qisheng Lu, *ibid.* **13**, 583 (2001) (in Chinese).